Available online at www.sciencedirect.com
SCIENCE DIRECT®
European Polymer Journal 41 (2005) 3011–3017
EUROPEAN POLYMER JOURNAL
www.elsevier.com/locate/europolj

Non-isothermal crystallization kinetics of exfoliated and intercalated polyethylene/montmorillonite nanocomposites prepared by in situ polymerization

Jun-Ting Xu *, Qi Wang, Zhi-Qiang Fan

Department of Polymer Science and Engineering, Zhejiang University, Hangzhou 310027, China

Received 21 December 2004; received in revised form 20 April 2005; accepted 20 April 2005
Available online 19 July 2005

Abstract

Polyethylene/montmorillonite (PE/MMT) nanocomposites, one intercalated sample with higher MMT content and one exfoliated sample with lower MMT content, were prepared by in situ polymerization using MMT-supported metallocene as catalyst. Non-isothermal crystallization behaviors of these two nanocomposites were investigated and compared. The exfoliated sample exhibits higher crystallization temperature (T_c) than the neat PE, showing nucleation effect of MMT. The intercalated sample has lower T_c than the neat PE due to the confinement of MMT. It is observed that the intercalated sample has longer induction period and faster overall crystallization rate, indicating co-existence of suppression and nucleation effects in this sample. The Avrami plots show that the crystal growth of PE in the intercalated sample is two-dimensional, while it is three-dimensional in the exfoliated sample. The crystallization activation energy of the intercalated sample is slightly smaller than that of the exfoliated sample.

Keywords: Differential scanning calorimetry (DSC); Crystallization; Nanocomposites; Polyethylene

1. Introduction

Polymer/clay nanocomposites usually have lots of improved properties when compared to the neat polymer, such as better mechanical properties, higher thermal stability, reduced thermal expansion coefficient and gas permeability [1,2]. For crystalline polymer/clay nanocomposites, crystallization behavior of the polymer is also affected by the clay. The addition of clay can change the crystallization kinetics, nucleation rate and even the crystal structure of the polymer [3–8]. In polymer/clay nanocomposites, the clay may exist in two forms: exfoliation or intercalation. In the exfoliated nanocomposites the distance between two clay layers is very large and the ordered lamellar structure of the clay is destroyed, while in the intercalated polymer/clay nanocomposites the lamellar structure of the clay is retained though the polymer inserts into the nanogalleries of the clay. The intercalated polymer/clay nanocomposites provide a model for studying the behavior of polymer confined in a two-dimensional space [9,10]. For example, it has been observed that crystallization of poly(ethylene oxide) (PEO) is greatly suppressed when PEO is confined in the clay layers [11,12]. However, so far most of the intercalated polymer/clay nanocomposites in literature usually contain low weight percentage

* Corresponding author. Tel./fax: +86 571 8795 2400.
E-mail address: xujt@zju.edu.cn (J.-T. Xu).

0014-3057/$ - see front matter © 2005 Elsevier Ltd. All rights reserved.
doi:10.1016/j.eurpolymj.2005.04.042

of clay and are prepared by melt or solution blending [13–15]. As a result, there are lots of polymers outside the clay layers though some of the polymers insert into the clay layers. Polymer/clay nanocomposites can also be prepared by in situ polymerization in the presence of initiator or catalyst supported into the clay galleries [16–23]. With this method, intercalation or exfoliation can be readily controlled by regulating the amount of polymer polymerized. In the present work, one intercalated PE/MMT nanocomposite with higher MMT content and one exfoliated PE/MMT nanocomposite with lower MMT content were prepared by in situ polymerization using MMT-supported metallocene catalyst. Non-isothermal crystallization behaviors of these two nanocomposites were investigated and compared.

2. Experimental

2.1. Preparation and characterization of the PE/MMT nanocomposites

Preparation of the nanocomposites has been described in Ref. [23]. The contents of PE in the nanocomposites were determined by extraction with xylene, and xylene-extractable polyethylene was subjected to gel permeation chromatography (GPC) characterization, which was performed on a PL GPC-220 in 1,2,4-trichlorobenzene at 150 °C using narrow polystyrene as the standard. The content of residual MMT in the nanocomposites was analyzed with a Perkin–Elmer Pyris-1 TGA as well. XRD analyses were performed using a Siemens D5000 diffractometer with Cu radiation (40 kV, 40 mA). Scanning was in 0.02° steps at a speed of 2°/min.

2.2. DSC experiments

DSC experiments were carried out in a Perkin–Elmer Pyris-1 instrument. About 4–5 mg of the sample was encapsulated in an aluminum pan. The samples were first kept at 200 °C for 5 min to erase the thermal history, then were cooled to room temperature at 2 °C/min, 5 °C/min, 10 °C/min and 20 °C/min, respectively. At last the samples were heated to melt at a rate of 10 °C/min. Both crystallization and melting DSC traces were recorded.

3. Results and discussion

3.1. Structure of PE/MMT nanocomposites

The structures of these two nanocomposites have been determined by WAXD, TEM in our previous work [24]. Here we only present some main evidences for the exfoliated structure of sample A and the intercalated structure of sample B. Firstly, compared with the sharp (0 0 1) reflection of neat MMT, the diffused WAXD peak of Zr-MMT (Fig. 1) shows that the metallocene catalysts are loaded into the MMT galleries, leading to less ordered *d*-spacing of the MMT layers. This agrees with the immobilization mechanism of the catalyst: The MAO reacts with the residual H_2O in the MMT layers and then forms ion pairs with metallocene. Secondly, in TEM experiments only aggregated MMT morphology is observed in sample B, indicating that there are few polymers outside the MMT layers. In contrast, exfoliated morphology is observed in the sample A. Thirdly, it is found that the PE in the sample B has higher molecular weight than the PE in the sample A (Table 1), though sample B is prepared at much shorter polymerization time. This is because polymerization takes place between the MMT layers at short polymerization time and the active sites are less exposed to chain transfer reagent. The MMT contents in these two nanocomposites are determined by extraction and TGA, respectively, and the results are given in Table 1. It is found that the MMT content determined by extraction is slightly higher than that from TGA, indicating that a small amount of PE chains are strongly absorbed by MMT and cannot be extracted by solvent. The WAXD patterns in the 2θ range of 2°–10° for Zr-MMT, samples A and B are shown in Fig. 1. One can see from Fig. 1 that after polymerization for 15 min, the lamellar structure of the MMT is still retained. However, after polymerization for 45 min, the (0 0 1) reflection from MMT basically disappears and only a small WAXD peak

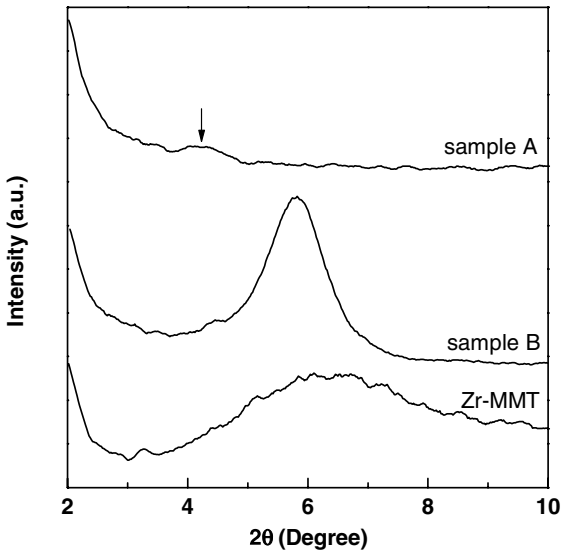

Fig. 1. WAXD patterns of Zr-MMT (supported catalyst), samples A and B.

Table 1
Polymerization time, MMT content, molecular weight and molecular weight distribution of PE/MMT nanocomposites

	Polymerization time (min)	MMT content (wt%)		M_n	M_w/M_n
		Extraction	TGA		
Sample A	45	11	10.2	4.4×10^4	2.6
Sample B	15	23	21.5	6.7×10^4	3.3

appears around $2\theta = 4°$. This shows that in the sample A most of the MMT layers are exfoliated and there are only a small amount of intercalated MMT layers. Even for the intercalated MMT layers in the sample A, the *d*-spacing is larger than that in the sample B.

3.2. Crystallization and melting behaviors

Fig. 2 shows the non-isothermal crystallization DSC curves of samples A and B at cooling rates of 2 °C/min and 10 °C/min, respectively. For the purpose of comparison, the DSC cooling trace of neat PE, which was obtained by extraction of the sample A, is given in Fig. 2(b) as well. It is found that at the cooling rate of 2 °C/min sample A exhibits a main crystallization peak together with a shoulder at lower temperature, while only single crystallization peak appears in the sample B. We notice that the lower temperature shoulder in sample A locates at the same position as the crystallization peak in the sample B. The WAXD pattern also shows that there is still a small amount of intercalated MMT in the sample A. Therefore, the lower temperature shoulder in the sample A may be ascribed to crystallization of the intercalated fraction. Fig. 3 summarizes the crystallization temperatures (T_c) and melting temperatures (T_m) of these two nanocomposites. It is observed that the intercalated sample B always exhibits lower T_c and T_m than the exfoliated sample A. This indicates that confinement of PE in the MMT layer suppresses crystallization of PE. Moreover, one can see from Fig. 2(b) that sample A has higher crystallization temperature (T_c) than the neat PE, showing the nucleation effect of MMT [5–7]. On the other hand, the intercalated sample

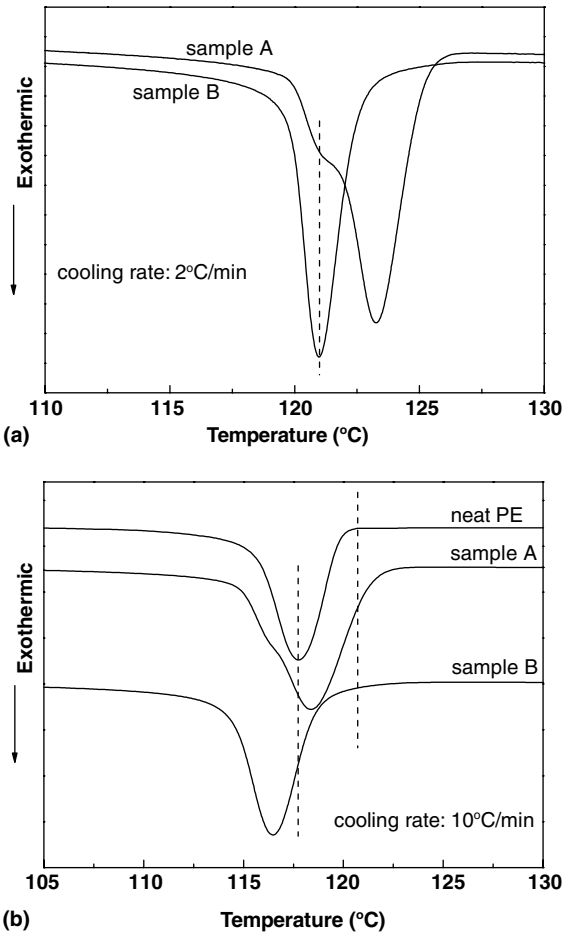

Fig. 2. Non-isothermal crystallization DSC curves of PE/MMT nanocomposites at the cooling rates of (a) 2 °C/min and (b) 10 °C/min.

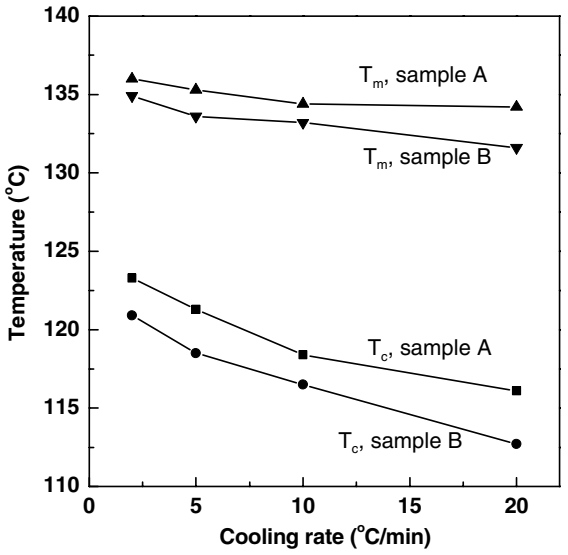

Fig. 3. Melting temperatures and crystallization temperatures of PE/MMT nanocomposites at various cooling rates.

B has lower crystallization temperature than the neat PE, which can be attributed to the confinement of MMT layers to PE crystals. Nevertheless, it is observed that both the exfoliated sample A and the intercalated sample B start to crystallize at higher temperature than the neat PE. As a result, we believed that MMT still have nucleation effect on crystallization of PE in the intercalated sample B and both nucleation and suppression effects co-exist in this sample.

Co-existence of suppression and nucleation effects is also reflected by the induction period and faster overall crystallization rate of the intercalated sample B. The changes of relative crystallinity with temperature and crystallization time are shown in Fig. 4. It is found that, although these two samples start to crystallize at similar temperature, the crystallinity of the intercalated sample B increases very slowly in the initial crystallization stage. One can see clearly from Fig. 4(b) that there is an induction period for crystallization of sample B. The overall crystallization rate is evaluated by the half-height width of crystallization peak ($\Delta T_{1/2}$). The larger value of $\Delta T_{1/2}$, indicates a slower crystallization rate. Fig. 5 shows the $\Delta T_{1/2}$ values of these two nanocomposites. It is found that the intercalated sample B has smaller $\Delta T_{1/2}$ than the exfoliated sample A at all cooling rates, indicating that the intercalated sample B crystallizes faster than the exfoliated sample A. Crystallization rate of a polymer is determined by the nucleation rate and mobility of polymer chains. As temperature decreases, the nucleation rate increases, while mobility of polymer chains decreases. At high temperature the number of nucleated polymer crystal embryos is small. If the mobility of polymer chains is simultaneously reduced, crystallization will progress very slowly. This is the situation in the induction period of the intercalated sample B, since the polymer chains are confined in a two-dimensional space and the polymer chains have lower mobility. At lower crystallization temperature, the intercalated sample B has faster nucleation rate than the exfoliated sample A because of its higher MMT content, and thus exhibits a faster overall crystallization rate.

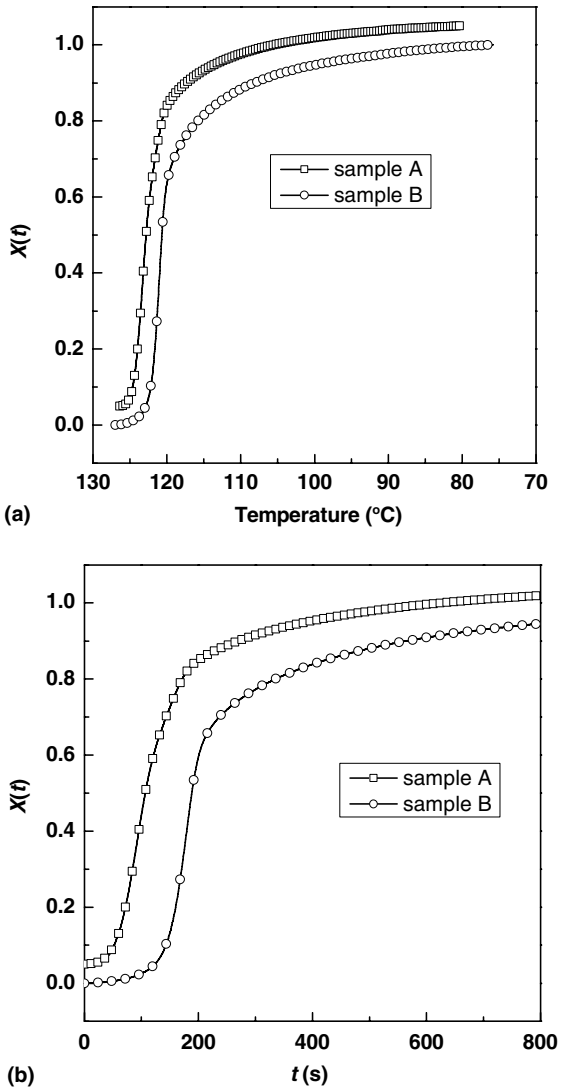

Fig. 4. (a) $X(t)$ versus temperature plots and (b) $X(t)$ versus crystallization time plots of PE/MMT nanocomposites at the cooling rates of 2 °C/min. The values of the sample A were shifted up 0.05 for clarity.

3.3. Non-isothermal crystallization kinetics

Avrami equation was modified by Jeziorny to describe the non-isothermal kinetics of polymer, although which is originally used for isothermal crystallization [25,26].

$$1 - X(t) = \exp(-Z_t t^n) \tag{1}$$

where the Avrami exponent n is a constant that depends on the type of nucleation and growth process parameters, and Z_t is a composite rate constant involving both nucleation and growth rate parameters. Jeziorny equation has been successfully applied to describe non-isothermal crystallization behaviors of many polymers and polymer composites [15,27–34]. Eq. (1) can be transformed into:

$$\ln[-\ln(1 - X(t))] = \ln Z_t + n \ln t \tag{2}$$

The Avrami exponent n and constant Z_t can be obtained from the slope and the interception in the plot of $\ln[-\ln(1-X(t))]$ against $\ln t$ at each cooling rate, respectively. When the parameter Z_t is corrected by the cooling rate ϕ, the reduced crystallization rate constant Z_c in non-isothermal crystallization is obtained:

$$\ln Z_c = \ln Z_t / \phi \tag{3}$$

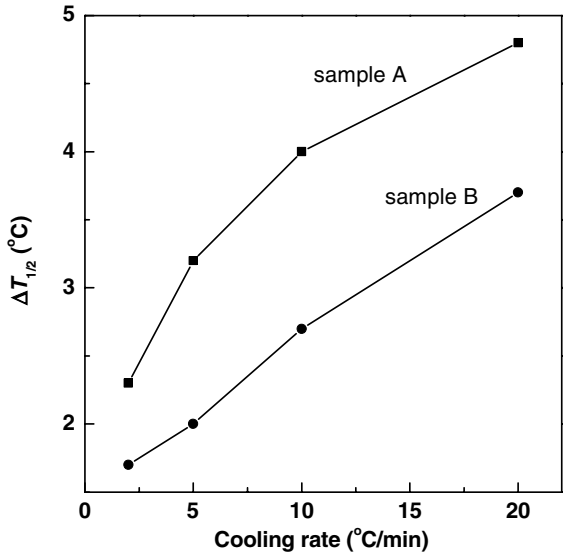

Fig. 5. Half-height width of crystallization peak ($\Delta T_{1/2}$) of PE/MMT nanocomposites at various cooling rates.

The Avrami plots for samples A and B at various cooling rates are shown in Fig. 6. It is found that the Avrami exponents for sample A are around 3.0, indicating a three-dimensional growth of the PE crystals. In contrast, the intercalated sample B has Avrami exponents close to 2.0 at various cooling rates, implying that the growth of PE crystals in B is two-dimensional. This shows that the PE crystals in sample B are confined between the clay layers. Considering the smaller *d*-spacing between the MMT layers and the melting temperature just slightly lower than that of normal PE, we can conclude that the PE stems in sample B are parallel to the MMT layers, but not perpendicular to the clay layers, as shown in Fig. 7.

Ozawa equation is also frequently used to treat non-isothermal crystallization kinetics [35]. The Ozawa equation is derived from Avrami equation by assuming that the non-isothermal crystallization process is composed of infinitesimally small isothermal crystallization steps. The expression of Ozawa equation is

$$1 - X(T) = \exp[-K(T)/\phi^m] \tag{4}$$

where $X(T)$ is the relative degree of crystallinity at temperature T, $K(T)$ is the cooling crystallization function, ϕ is the cooling rate, and m is the Ozawa exponent and relative to the mechanism of nucleation and dimension of crystal growth. The double-logarithmic form of Eq. (4) is

$$\ln[-\ln(1 - X(T))] = \ln K(T) - m \ln \phi \tag{5}$$

If Ozawa equation is applicable to describe non-isothermal crystallization process, a linear relationship should be yielded when $\ln[-\ln(1 - X(T))]$ is plotted against

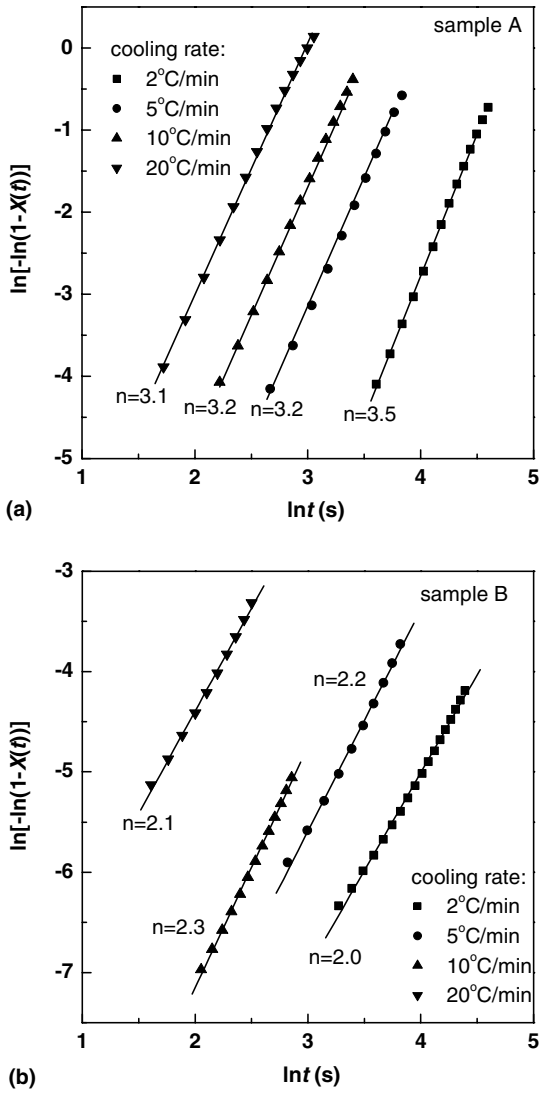

Fig. 6. Avrami plots for (a) sample A and (b) sample B.

$\ln \phi$. However, we failed to get a linear plot for both samples when Ozawa equation was applied. Possible reason is that no secondary crystallization is assumed in Ozawa's theory. Nevertheless, the overlapped crystallization temperature range at various cooling rates corresponds to the early crystallization stage at large cooling rate, but it corresponds to the late crystallization stage at small cooling rate. As is well known, secondary crystallization frequently occurs in the late crystallization stage.

Recently, Mo developed a new approach to non-isothermal crystallization of polymer [36]. There is following relationship among crystallization time t, cooling rate ϕ and crystallization temperature T:

$$t = (T_i - T)/\phi \tag{6}$$

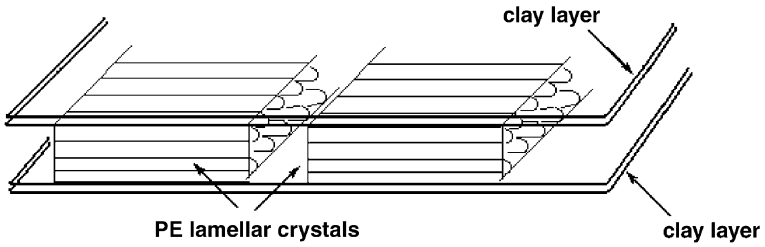

Fig. 7. Schematic for PE crystals intercalated between the MMT layers.

In combination with Eqs. (2), (5), and (6), following equation can be derived:

$$\ln\phi = \ln F(T) - \alpha \ln t \tag{7}$$

where $F(T) = [K(T)/Z_t]^{1/m}$ means the necessary cooling rate when the measured system reaches a certain crystallization degree at unit crystallization time, α is the ratio of Avrami exponent to Ozawa exponent, i.e. n/m. The plots of $\ln\phi$ against $\ln t$ for samples A and B at various crystallinity degrees are shown in Fig. 8. It is observed that all plots give a straight line, showing that this approach is applicable in the present work. The values of $F(T)$ and α, obtained form the interception and slope, respectively, are listed in Table 2. It is found that exfoliated sample A has smaller values of $F(T)$ than the intercalated sample B. This means that sample A can reach the same crystallinity degree at higher temperature than B and $F(T)$ mainly reflects the suppression effect of MMT on crystallization of PE. The values of α for both samples are basically constant at different crystallinity degrees, showing that Avrami exponent and Ozawa exponent change with crystallinity in a similar way.

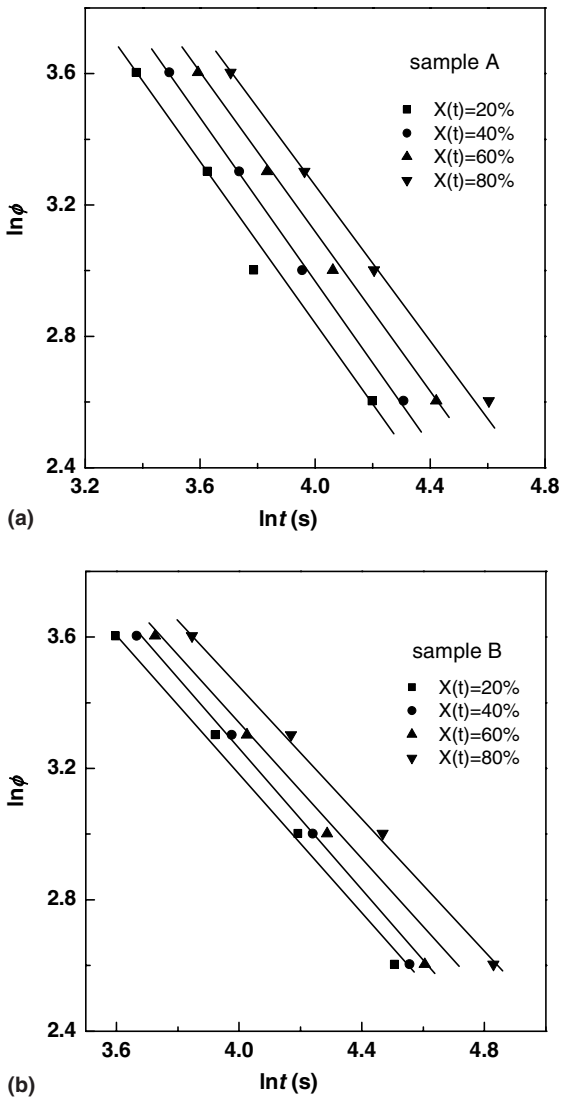

Fig. 8. Plots of $\ln\phi$ versus $\ln t$ for (a) sample A and (b) sample B.

Kissinger proposed a method to calculate activation energy in non-isothermal crystallization [37].

$$\frac{\mathrm{d}[\ln(\phi/T_c^2)]}{\mathrm{d}(1/T_c)} = -\frac{\Delta E}{R} \tag{8}$$

where R is the universal gas constant and ΔE is the activation energy of crystallization. The plots of $\ln(\phi T_c^2)$

Table 2
Values of $F(T)$ and α for the exfoliated and intercalated PE/MMT nanocomposites

Sample	$X(t)$ %	$F(T)$	α
A	20	398	1.23
	40	575	1.23
	60	691	1.20
	80	832	1.11
B	20	562	1.10
	40	708	1.12
	60	871	1.14
	80	977	1.06

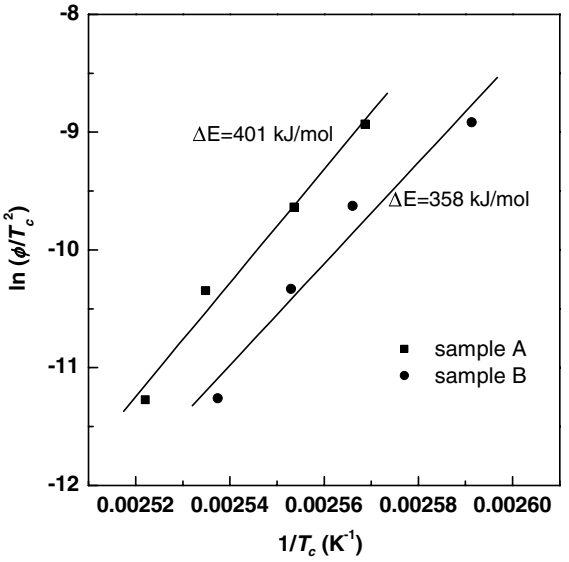

Fig. 9. Plots of $\ln(\phi/T_c^2)$ versus $\ln 1/T_c$ for samples A (■) and B (●).

against $1/T_c$ for samples A and B are depicted in Fig. 9. The crystallization activation energies were calculated from the slopes. It is found that the values of crystallization activation energy are 401 kJ/mol and 358 kJ/mol for samples A and B, respectively. The smaller energy barrier of crystallization for the intercalated sample B is in accordance with its faster overall crystallization rate.

4. Conclusions

The results reveal that the MMT has nucleation effect on crystallization of PE, leading to higher T_c of the exfoliated sample. However, the intercalated sample has lower T_c than the neat PE due to confinement of the MMT layers. The longer induction period, and faster overall crystallization rate of the intercalated sample show co-existence of nucleation and suppression effects. The Avrami analysis modified by Jeziorny and the method developed by Mo are applicable to describe the non-isothermal crystallization process of the intercalated and exfoliated PE/MMT nanocomposites prepared by in situ polymerization. The Avrami exponents are 2 and 3 for the intercalated and exfoliated samples, respectively. This indicates that the crystal growth is two-dimensional in the intercalated sample, while it is three-dimensional in the exfoliated sample. The activation energy for crystallization of PE in the intercalated sample is slightly smaller than that in the exfoliated sample.

References

[1] Gopakumar TG, Lee JA, Kontopoulou M, Parent JS. Polymer 2002;43:5483.
[2] Ray SS, Okamoto M. Macromol Rapid Commun 2003;24:815.
[3] Krikorian V, Pochan DJ. Macromolecules 2004;37:6480.
[4] Liu XH, Wu QJ, Berglund LA. Polymer 2002;43:4967.
[5] Ke YC, Yang ZB, Zhu CF. J Appl Polym Sci 2002;85:2677.
[6] Ma JS, Zhang SM, Qi ZN, Li G, Hu YL. J Appl Polym Sci 2002;83:1978.
[7] Pozsgay A, Frater T, Papp L, Sajo I, Pukanszky B. J Macromol Sci-Phys 2002;B41:1249.
[8] Ou CF, Ho MT, Lin JR. J Polym Res-Taiwan 2003;10:127.
[9] Giannelis EP, Krishnamoorti R, Manias E. Adv Polym Sci 1999;138:107.
[10] Manias E, Chen H, Krishnamoorti R, Genzer J, Kramer EJ, Giannelis EP. Macromolecules 2000;33:7955.
[11] Waddon AJ, Petrovic ZS. Polym J 2002;34:876.
[12] Kuppa V, Menakanit S, Krishnamoorti R, Manias E. J Polym Sci Part B: Polym Phys 2003;41:3285.
[13] Park CI, Park OO, Lim JG, Kim HJ. Polymer 2001;42:7465.
[14] Hu XB, Lesser AJ. J Polym Sci Part B: Polym Phys 2003;41:2275.
[15] Xu WB, Liang GD, Zhai HB, Tang SP, Hang GP, Pan WP. Eur Polym J 2003;39:1467.
[16] Tudor J, Ohare D. Chem Commun 1997:603.
[17] Weimer MW, Chen H, Giannelis EP, Sogah DY. J Am Chem Soc 1999;121:1615.
[18] Heinemann J, Reichert P, Thomann R, Mulhaupt R. Macromol Rapid Commun 1999;20:423.
[19] Jin YH, Park HJ, Im SS, Kwak SY, Kwak S. Macromol Rapid Commun 2002;23:135.
[20] Ke YC, Long CF, Qi ZN. J Appl Polym Sci 1999;71:1139.
[21] Kuo SW, Huang WJ, Huang SB, Kao HC, Chang FC. Polymer 2003;44:7709.
[22] Yang F, Zhang XQ, Zhao HC, Chen B, Huang BT, Feng ZL. J Appl Polym Sci 2003;89:3680.
[23] Wang Q, Zhou ZY, Song LX, Xu H, Wang L. J Polym Sci Part A: Polym Chem 2004;42:38.
[24] Xu JT, Zhao YQ, Wang Q, Fan ZQ. Macromol Rapid Commun 2005;26:620.
[25] Avrami M. J Chem Phys 1939;7:1103.
[26] Jeziorny A. Polymer 1978;19:1142.
[27] Liang GD, Xu JT, Xu WB. J Appl Polym Sci 2004;91:3054.
[28] Xu JT, Xue L, Fan ZQ. J Appl Polym Sci 2004;93:1724.
[29] Canetti M, De Chirico A, Audisio G. J Appl Polym Sci 2004;91:1435.
[30] Gao JG, Yu MS, Li ZT. Eur Polym J 2004;40:1533.
[31] Weng WG, Chen GH, Wu DJ. Polymer 2003;44:8119.
[32] Chen C, Fei B, Peng SW, Zhuang YG, Dong LS, Feng ZL. Eur Polym J 2002;38:1663.
[33] Qiu ZB, Mo ZS, Zhang HF, Sheng SR, Song CS. J Macromol Sci-Phys 2000;B39:373.
[34] An YX, Li LX, Dong LS, Mo ZS, Feng ZL. J Polym Sci Part B: Polym Phys 1999;37:443.
[35] Ozawa T. Polymer 1971;12:150.
[36] Liu TX, Mo ZS, Wang SE, Zhang HF. Polym Eng Sci 1997;37:568.
[37] Kissinger HE. J Res Natl Bur Stand 1956;57:217.